2. The investigated material: Calcium fluoride

The aim of this chapter is to make the reader familiar with the ionic crystal Calcium fluoride, and to emphasize some specific features of this material that are important in the context of this work. In the first part, the geometrical and electronic structure of the pure material is introduced. This section is followed by a survey of irradiation induced defects in CaF_2 and a description of the development of these defects into colloids. Then, some effects are described which are related to electron and photon irradiation that are not specific to CaF_2. The issues here are the penetration depth of primary electrons and the mean free path of photoelectrons.

2.1. Structure of the CaF_2 crystal

CaF_2 is an ionic crystal with the fluorite structure. The lattice is a face centered cubic (fcc) structure with three sublattices. The unit cell of the material is most easily described as a simple cubic lattice formed by the F^- ions where a Ca^{2+} ion is contained in every second cube. The remaining empty cubes (called interstitial or hollow sites) are important for defect formation and diffusion, but also for the accommodation of unwanted impurities like rare earth ions and dopants. The lattice constant is a=5.451 Å [JCh83] (Fig. 2.1). The natural cleavage plane of the crystal is the (111) surface. It is build up from F^--Ca^{2+}-F^- triple layers of 3.14 Å distance and is terminated by fluorine ions. In Fig. 2.1, the four possible (111) planes are defined by

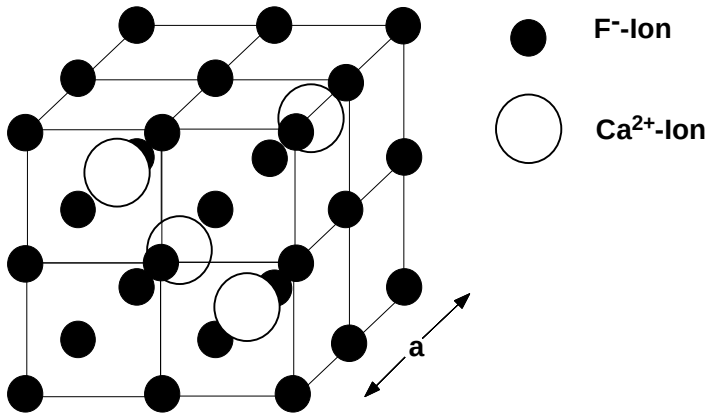

Fig. 2.1 The unit cell of CaF_2. The lattice constant is a = 5.451 Å. The position of the fluoride ions is marked by black spheres, the position of the Ca^{2+} ions by white spheres. The Calcium ions are surrounded by eight neighboring fluoride ions, while the fluoride ions are surrounded by a tetrahedron of four calcium ions. Note that in the resulting structure every alternate cube of fluoride ions has no calcium ion in its center. The (111) plane is the natural cleavage plane of the crystal, in this picture, it is defined by each triple of the four Ca^{2+} ions. The ionic radii are 0.99 Å for Ca^{2+} and 1.36 Å for F^- [Kit91].

each respective triple of the four Ca^{2+} ions. The melting point of CaF_2 is at 1620 K. At a temperature of 1420 K, a maximum of the specific heat is observed that is caused by melting of the fluorine sublattice. The fluorine ions are randomly distributed over the normal lattice sites (tetrahedrally coordinated) and the interstitial sites (octahedrally coordinated). The ionic mobility consequently becomes very high. The behavior is known as superionic conduction, it is observed in a variety of materials with the fluorite structure [Hay74].

CaF_2 has a wide bandgap of about 12 eV, values in literature range from 11.6 eV [BJC90] to 12.1 eV [Rub72]. The first exciton peak is at 11.2 eV. The band structure was calculated by a number of authors [AJG77], [HLi80], [SSA81], [GXH92]. The valence band of CaF_2 consists of 2p levels of the fluorine ions, while the bottom of the conduction band originates from the 4s and 3d orbitals of the calcium ions.

The influence of structural relaxation on the surface electronic structure of CaF_2 was calculated by Stankiewicz and Modrak [SMo95]. Only very small effects were found. The electronic structure of the perfect (111) surface and several low index stepped surfaces were calculated

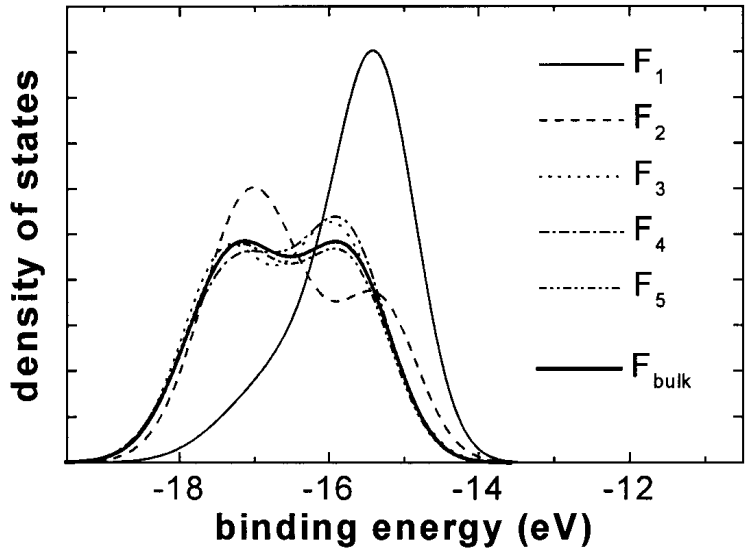

Fig. 2.2 Projected density of states in the F2p valence band for different F^- ions. The solid line represents the bulk density of states (picture taken from [PPH98]). The labels F_1 to F_5 denote the density of states in several fluorine layers, starting from the upper surface layer F_1.

by V. Puchin [PPH98] with the Hartree-Fock method. Differences between bulk and surface valence band structure were found (see Fig. 2.2). At the stepped surface, the band gap was reduced by about 0.5 eV.

The existence of surface excitations in fluorides was experimentally demonstrated by Saiki et al [SXK92] with low energy electron loss spectroscopy. In their study, the energy loss spectra of several alkali and alkaline earth halogenides were compared. Only for fluoride materials, a distinct peak with an energy lower than the lowest excitation found in optical reflectivity spectra or high energy electron loss spectroscopy was observed (see table 2.1).

material	Peak position in low-energy EELS (eV)	Peak position in high-energy EELS (eV)	Peak position in optical reflectivity (eV)
LiF	10.2		
	13.4	13.5	12.4
NaF	9.2		
	11.1	10.9	10.5
CaF_2	10.0		
	11.8, 13.2	11.8, 13.2	11.1, 13.0
SrF_2	9.3		
	10.9, 12.2	10.8, 12.2	10.4, 12.0
BaF_2	8.9		
	10.6, 12.9	11.0, 13.8	9.8, 12.5
LiCl	8.0, 9.8	8.8, 9.8	8.6, 9.5
NaCl	7.8, 10.3	8.1, 10.2	7.8, 10.0
LiBr	7.0, 8.4	7.1, 8.4	7.0, 7.7, 9.7
NaBr	6.6, 7.1, 8.6	6.6, 7.1, 8.8	6.5, 7.1, 8.6

Tab. 2.1 Peak energies of excitations in a number of alkaline and alkaline earth halogenides measured with low-energy EELS (150 eV), high-energy EELS (50 keV) and optical reflectivity. A well resolved surface excitation is observed for fluorides only. Data from [SXK92].

The intensity of this peak decreased with increasing primary energy. It was therefore attributed to a surface excitation. Saiki et al [SXK92] interpreted the surface excitation as a transition of electrons from the valence band to a low lying surface state originating from the metal ions. Similar surface excitations had been observed earlier by Cox and Williams [CWi86] on LiF and MgO, but not on NaCl and KBr. These authors concluded that a surface excitation exists for materials where the conduction band edge is above the vacuum level. The final state of the excited electron is located outside the surface with an energy close to the vacuum potential. The electron was assumed be bound by its image potential with an additional contribution from the valence band hole. The result is a series of Rydberg states with binding energies of several tenth of an eV.

2.2 Defects and surface defects in CaF_2

In this section, defects in CaF_2 that can be produced by electron or UV light irradiation are discussed. The defects are confined to the anion sublattice, while the cation sublattice remains unaffected. This can be understood from the large difference in formation energy of anion Frenkel pairs (2.6 - 2.7 eV) and cation Frenkel pairs (8.5 - 9.2 eV) [CNo73]. Defects can be neutral or charged, the latter species are responsible for the increased electrical conductivity during irradiation and for field enhanced diffusion phenomena. A defect is considered neutral if the unit cell containing the defect remains neutral. In the electron and photon energy regime used in this work, defects are produced by electronic excitation only and not by displacement due to momentum transfer. The first basic step of defect creation is a bandgap excitation of an electron - hole (e-h) pair by ionizing radiation. As an estimate for the energy loss of the primary electrons per e-h excitation, Alig and Blohm gave a value of about three times the bandgap energy [ABl75]. Due to Coulomb attraction, the electron hole pairs form excitons. CaF_2 is a material with strong electron-phonon coupling [KOI95], in which excitons localize by means of a lattice deformation to form self-trapped excitons (STE). This process occurs within picoseconds and has an efficiency of almost 1 [SWi93]. The possible configurations of the STE in CaF_2 are shown in Fig 2.3.

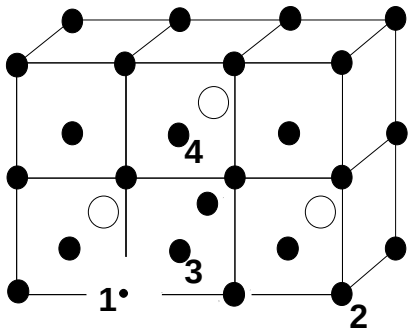

Fig. 2.3 The self-trapped exciton in CaF_2. Other possible configurations of this defect can be obtained by interchanging the position of the *F*-center with the fluoride ions on the positions 2 to 4.

One of the fluoride ions releases an electron and moves into one of the empty cubes. A covalent bond is established to one of the neighboring fluorides on a regular lattice site, thus a H-center (F_2^-, see below) is formed. The electron localizes on the vacant lattice site to form a *F*-center. The electronic state of the STE is a metastable $^3\Sigma_g$ state, which is schematically depicted in Fig. 2.4. Two optical absorption bands have been reported. At 3 eV, the *F*-center is

excited, while the other band centered around 4.1 eV belongs to a hole excitation of the H-center. At this energy, the hole is excited from the top antibonding σ_u orbital of the F_2^- molecular ion to the binding σ_g orbital, compare Fig. 2.4. Both excitations are slightly shifted

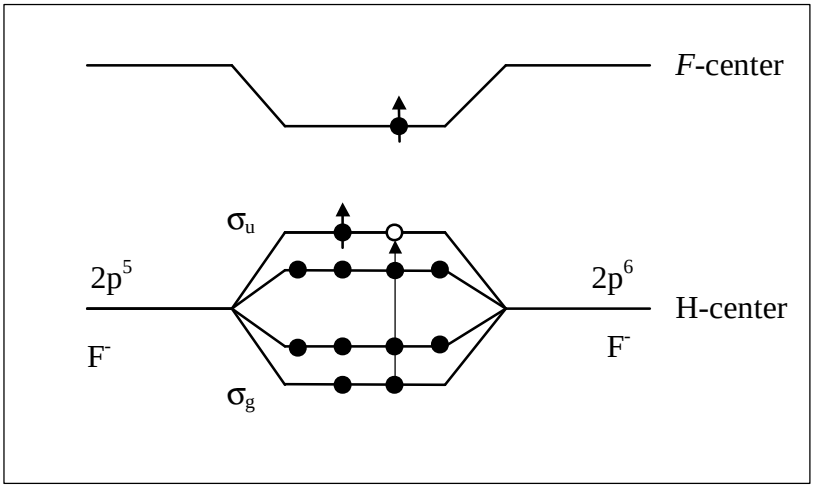

Fig. 2.4 Electronic structure of the metastable $^3\Sigma_g$ state of the self-trapped exciton. The absorption band of the *F*-center is at 3 eV, the excitation at 4.1 eV that is marked by an arrow corresponds to the excitation of the hole (open circle) from the σ_u to the σ_g level of the F_2^- molecular ion (= H-center).

compared those of the free defects (see below). The lifetime of the metastable $^3\Sigma_g$ state of the STE is 1.7 µs at room temperature (RT). Three decay channels of the STE where observed. At low temperature, mainly a radiative decay takes place. The STE recombines into the ground state under emission of a broad luminescence band centered at 4.4 eV. The remaining elastic deformation is removed by the excitation of phonons. With increasing temperature, non-radiative recombination into the undisturbed lattice becomes important.

In the context of the present work, the third decay channel is the most interesting: separation of the STE into *F* and H-centers. Stable defects, that do not recombine as easily as the STE, are produced. Separation can be thermally activated, thus the efficiency of metal production is higher at elevated temperature [Bou97]. Also the excitation of the H-center at 4.1 eV results in a dissociation of the STE [TKI89] (solid arrow in Fig 2.4.). The neutral fluorine can move to the next neighbor cube where again a H-center is formed by bonding to a fluoride ion on a regular lattice point. Also excitation with electrons, as was carried out in this work, was found to results in stable defects. Point defects in crystals with the fluorite structure have been reviewed by Hayes [Hay74]. The following brief description of the most prominent defects in CaF_2 given below has been extracted mainly from this work.

***F*-center** The *F*-center is a fluoride ion vacancy binding one electron. It is shown schematically in Fig. 2.5. To avoid confusion with F denoting fluorine, the *F*-center is written as an italic letter throughout this work.

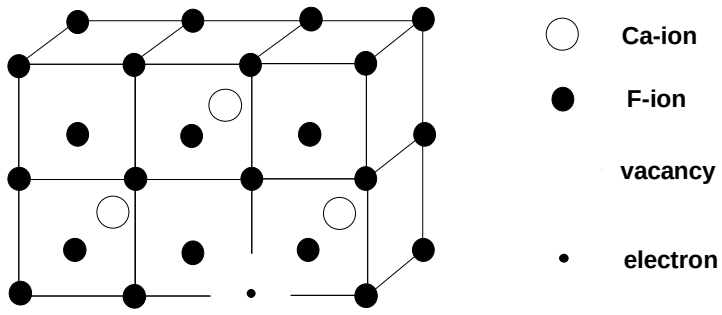

Fig. 2.5 Configuration of the *F*-center in CaF_2. An electron is localized in a fluorine vacancy. This defect is neutral.

The electronic structure of the *F*-center was investigated by Stoneham et al [SHS68]. It was shown that the ground state of the 1s wave function of the *F*-center is restricted to the anion vacancy. As the *F*-center is slightly larger than the fluorine ion, the cations move outwards by 4.2 % [Hay74]. The peak of the absorption band is at 3.3 eV with 0.3 FWHM [CHH69] and corresponds to an excitation from the 1s state to the 2p state. The 2p state, however, is already quite delocalized. Two neighboring *F*-centers form a M-center, three a R-center. A larger cluster of *F*-centers constitutes an area in the crystal that is free of fluorine. Metallic colloids can therefore be formed by *F*-center diffusion. In CaF_2, this process is favored because the lattice constant of the Ca fcc sublattice (5.451 Å) is very similar to the fcc lattice constant of Ca metal (5.58 Å [AMe76]). No reliable data are known for the *F*-center diffusion constant and energy. The annealing of *F*-centers in CaF_2 following neutron irradiation at 20 K has been investigated by Atobe [Ato79]. Three steps of *F*-center decay were observed: the first with an activation energy of 0.33 eV was attributed to the recombination of *F*-centers with thermally activated V_K-centers. The second step with an activation energy of 0.46 eV was assumed to be due to H-centers. The remaining *F*-centers decay with an activation energy of 0.72 eV. A mechanism for this last step was not proposed by Atobe, however, it follows that the *F*-center activation energy is 0.72 eV if the last step is due to *F*-center mobility, or larger if other defects become mobile and recombine with the remaining *F*-centers.

H-center A H-center in CaF_2 is an interstitial fluorine atom covalently bonded to a fluorine ion on a normal lattice site. The bond is along the ⟨111⟩ crystal axis (see Fig. 2.6.) The peak of the optical absorption band is at 4 eV, a value for the activation energy for diffusion of 0.46 eV was given by Atobe [Ato79].

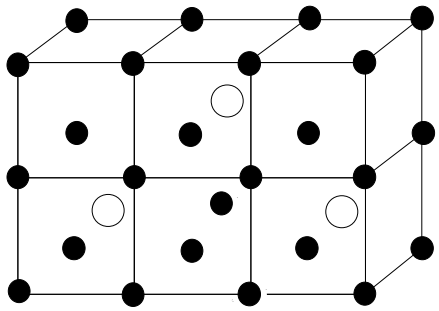

Fig. 2.6. Configuration of the H-center in CaF_2. The fluorine atom in the center of the cube is bonded covalently to one of the fluoride ions on the edges of the cube. This is a neutral defect.

I-center A negative fluoride ion residing in the center of an interstitial site is called an I-center. The defect may be produced by ionization of a H-center, as a charge compensating defect if the crystal is doped with three-valent rare earth ions, or by formation of an anion vacancy by thermal excitation (anion Frenkel pair). As the I-center consists of a filled shell ion, no covalent bonds to the neighboring ions on the regular lattice sites are formed. The I-center is not paramagnetic and no optical transitions have been reported. Only the perturbing influence on *F*-centers manifests its existence. Diffusion energies ranging from 0.53 to 1.63 eV have been reported in [Hay74] and of 1 eV in [Twi71]. The I-center can be easier ionized than a regular fluoride ion as the Madelung potential in the center of the cube is negative. Since it is a charged defect, no I-center clusters are to be expected. By recombination with a V_K-center, the I-center is converted to a H-center.

Anion vacancy The anion vacancy is a positively charged defect. It is created together with an I-center by thermal excitation (anion Frenkel pair) or exists in CaF_2 as a charge compensating defect if the crystal is doped with monovalent alkali metal ions. Also electron stimulated desorption of fluorine produces vacancies at the surface. The measured activation energies for diffusion range from 0.52 to 0.87 eV. Due to its lower activation energy, the vacancy is more efficient in charge transport than the I-center. This situation is opposite to that encountered in most other solids, where the anion vacancy is less mobile than the corresponding interstitial.

V_K-center The self-trapped hole in CaF_2 consists of a F_2^- molecular ion with the bond axis oriented parallel to the ⟨100⟩ axis. It is formed during photoemission from valence band holes, or it may be produced together with an I-center from a H-center. A drawing of this defect is shown in Fig. 2.7.

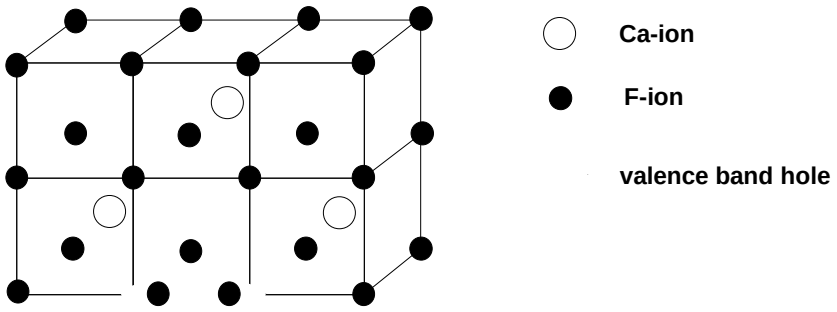

Fig. 2.7. The V_K-center in CaF_2. This positively charged defect may be described as a F_2^- molecular ion with the bond axis parallel to the ⟨100⟩ direction.

The maximum of the absorption band is at 3.9 eV. Excitation energies for diffusion along the ⟨100⟩ axis ranging from 0.2 to 0.5 eV have been reported in [Hay74], of 0.3 eV in [BHK70] and of 0.33 eV in [Ato79]. The self-trapped hole plays an important role in increasing the electrical conductivity of CaF_2 during photon irradiation where also an activation energy of about 0.3 eV was determined (compare Chapter 5).

Surface *F*-center From the intrinsic defects described in the preceding part, only *F*-centers and vacancies are known to exist at the surface. For the *F*-center, electron energy loss spectroscopy measurements yields an excitation energy of 1.8 eV [SSK87]. The ground state of the surface *F*-center lies 8.3 eV above VBM, as was concluded from photoemission results [KHM86], [RHK87]. The energetic position of surface *F*-center states has been investigated in the molecular cluster calculation of Westin et al [WRM90]. For a single *F*-center, a state 2 eV below the vacuum level was found, while for clusters of three *F*-centers, the binding energy was in the range of 1.4 to 1.9 eV.

2.3 Defect aggregation: Metal colloids

At sufficiently high temperature, point defects are mobile and neutral species are able to form larger clusters. During ionizing irradiation, part of the fluorine diffuses to the surface and desorbs, but no metal desorption is observed for temperatures below about 600 K. For this reason, after irradiation an excess of metal is present in the surface layers of the crystal down

to the penetration depth of the incident beam. It has already been pointed out that a large number of aggregated *F*-centers are equivalent to metallic colloids. *F*-center clustering in CaF_2 exhibits some specific features that are due to the similarity of the Ca sublattice in CaF_2 to the lattice of Ca metal. Both lattices are face centered cubic with a mismatch of only 2%. A similar situation is encountered in SrF_2, except here the lattice mismatch is about 4%. In all other alkali and alkaline earth halides, the structures of the cation sublattice differ from the metal lattice. Metallic colloids are therefore the most prominent clusters found in CaF_2. The size of alkaline earth metal colloids in the fluorides can be as large as 10 µm, which is much larger than colloids observed in alkali halides. These large clusters can be investigated with optical microscopy, and were found to have well defined crystal structures [HJa79]. Bulk colloid formation after electron irradiation has been investigated with electron spin resonance [MEv68], optical spectroscopy [AOr76], [Bou97], [HBR98], and electron microscopy [JCh83]. For the spin resonance measurements, CaF_2 was irradiated with electrons of 75 keV energy. After irradiation, resonance lines typical for conduction band electrons were found, and results indicated the formation of Ca clusters with a radius below 30 nm [MEv68]. Lower excitation energies have been used for colloid production in [Gün94], [Bou97], [HBR98]. Irradiation of the crystals was performed at about 190 K with electrons of 1.0 to 3.0 keV primary energy at dosages between 90 and 360 mC/cm^2. While the crystal was slowly heated at a rate of typically 1 K/min, optical absorption spectra were taken (Fig 2.8).

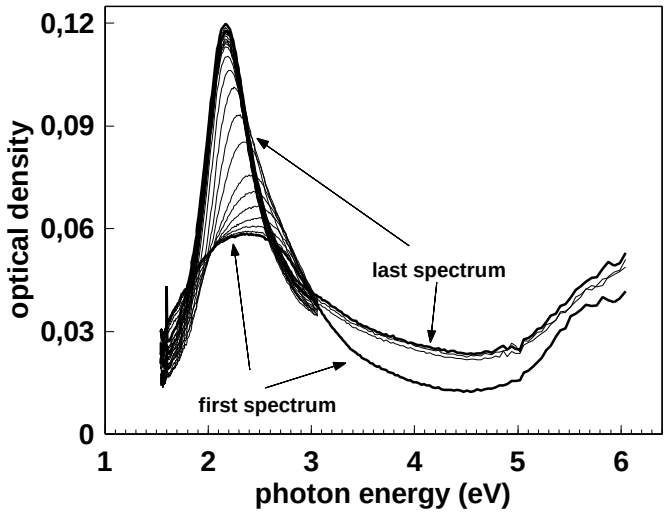

Fig. 2.8 Series of optical spectra taken during heating after irradiation at 192 K according to [Bou97]. The two solid lines mark the first (at 200 K) and the last (at 370 K) recorded spectrum. In the first spectrum taken after electron irradiation, only two broad features centered at 2.3 and 6 eV are found. Note that no isolated defects like *F*-centers (at 3.3 eV) are distinguishable. Irradiation parameters: 2.5 keV 175 mC/cm^2 T=192 K Heating rate: 1.17 K/min. [Bou97]

After irradiation, two broad bands were observed. The first at a position of 2.3 eV was interpreted as optical extinction caused by small colloids of about 1 nm radius. The feature at 6 eV could not be assigned to any intrinsic defect, as a speculative explanation, oxygen impurities were considered. Surprisingly, no isolated defect bands were found, in contrast to the situation observed with LiF after irradiation with the same dose [Bou97]. This is even more remarkable as LiF is much easier to colorate than CaF_2, the beam induced density of defects is much higher in the former material. Technical improvements introduced in the present work made it promising to repeat some of these experiments with vacuum cleaved crystals to check the hypothesis whether the band at 6 eV is due to oxygen, and at lower irradiation temperature to see if isolated defects could be observed. The results can be found in chapter 6. From the position of the low energy absorption band in Fig. 2.8, the radius of the colloids was determined with Mie theory. The results of the measurement are shown in Fig. 2.9. Starting from a radius of about 1 nm at low temperature, a steplike growth around 270 K was observed that in this experiment finally resulted in stable colloids of about 22 nm radius.

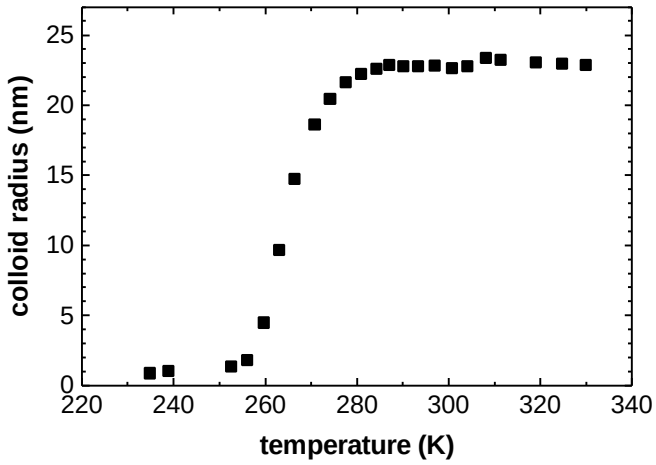

Fig. 2.9 Development of colloid radii during heating after irradiation at 192 K. Irradiation parameters were: 2.5 keV beam energy, 175 mC/cm^2 electron dose density, T=192 K irradiation temperature. Heating rate: 1.17 K/min. [Bou97]

A series of these experiments have been conveyed to reveal the parameters influencing the final colloid radius after heating. It could be shown that the crucial parameter determining the colloid size was the sample temperature during electron irradiation (Fig 2.10), while no dependence of the irradiation dosage could be detected. The primary electron energy may have

a small influence, as the reduced penetration depth at low energy may prevent the formation of larger colloids [Bou97].

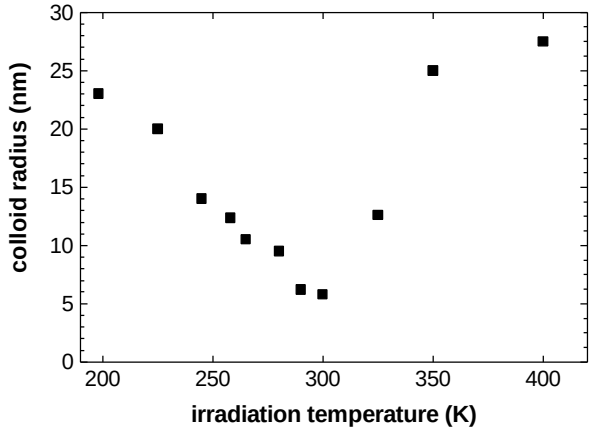

Fig. 2.10 Dependence of the final colloid radius on irradiation temperature. The final colloid radius has a minimum for an irradiation temperature of about 300 K. Higher as well as lower irradiation temperature resulted in much larger colloids. Irradiation parameters: 2.5 keV, 60 µA/cm^2 Colloid radii were determined at 370 K [Bou97].

The final colloid radius was found to decrease from about 25 nm for irradiation at 190 K to 6 nm for irradiation at 300 K. For higher irradiation temperatures, colloid radii were observed to increase again (Fig. 2.10). So far, no explanation is known for this temperature dependence.

2.4. Stopping power and penetration depth of low energy electrons in CaF_2

The stopping power of low energy electrons in CaF_2 has been calculated by N. Itoh during his guest stay in our group. The calculation followed the model proposed by Ashley [Ash88] using data from optical absorption experiments. This model provides a simple way of extending the

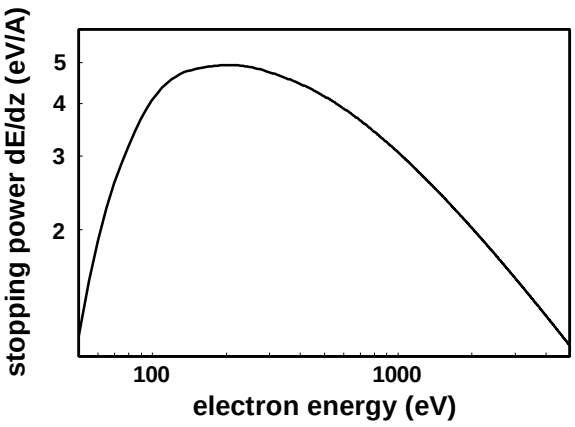

Fig. 2.11 Stopping power of CaF_2 as calculated from optical data [BSR95].

imaginary part of the dielectric function without momentum transfer to the dielectric function with finite momentum transfer. As the optical data are available for a limited energy range only (below 36 eV), an extrapolation procedure using the power relation for the optical reflectivity $k\omega^{-4}$ (where k is a constant, and $\hbar w$ the photon energy) was necessary. The results of this calculation are shown in Fig. 2.11. The maximum value of the stopping power is approximately 5 eV/Å at an electron energy of 200 eV.

The stopping power values obtained by N. Itoh have been used by R. Bennewitz [BSR95] as an input to perform a Monte Carlo calculation of the energy deposition curves dE/dz. The calculation was carried out using the method suggested by Scott and Love [SLo83]. The simulation was stopped when the electron kinetic energy dropped below 36 eV. The result is shown in Fig. 2.12 for three primary energies. The penetration depth as a function of primary

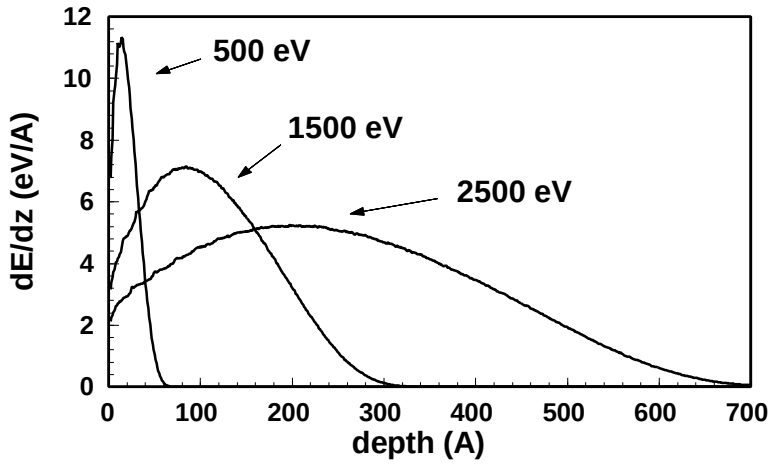

Fig. 2.12 Calculated energy deposition curves for incident electron energies 0.5, 1.5 and 2.5 keV [BSR95].

electron energy can be described by the simple power law D = 190 Å $(E_{primary}/keV)^{1.45}$. The peak of the energy deposition is at 25 % of the maximum penetration depth for primary electron energies above 0.8 keV, while it is less than 25 % for lower primary energies.

By experimental investigations, it was shown that the penetration depth of low energy electrons can be very large in wide bandgap materials. Quiniou et al [QSW92] investigated photoemission excited with near UV laser light from Si through overlying epitaxial layers of CaF_2. While for amorphous layers, the attenuation length is in the order of typically 100 Å, for the epitaxial layers, an attenuation length of 2600 Å was determined. Electron emission was observed even through overlayers as thick as 8000 Å. These results probably also imply that electrons excited to the conduction band of CaF_2 are not easily selftrapped, in contrast to holes created in the valence band, where selftrapping occurs very fast.

2.5 Mean free path in insulators

In the preceding section 2.4, we where concerned with the maximum range of electrons in a crystal. In addition, for photoelectron spectroscopy it is important to have an estimate of the sampling depth of the experiment, which is about the average distance a photoexcited electron can travel before it is scattered for the first time and the information of the initial energy is lost. This distance is called the mean free path of an electron with a certain kinetic energy. It was found that the energy dependence of the mean free path can be described by an universal curve that is quite generally applicable to a large variety of materials. The minimum of this curve is about 3 Å at kinetic energies between 40 and 100 eV, with a slow increase towards higher kinetic energies (Fig. 2.13). For energies lower than the universal minimum, a different

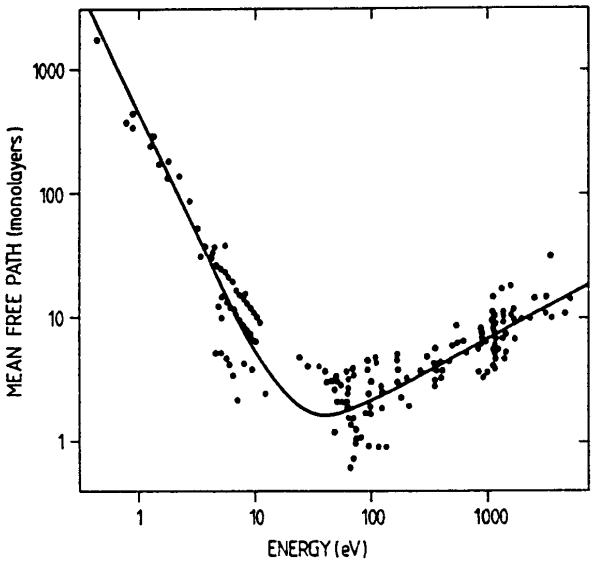

Fig. 2.13 Universal curve for the mean free path of electrons in solids [Lüt95]. For energies below about 10 eV, insulators have much larger mean free paths than indicated by this curve due to the less effective loss mechanism for electron energies below the bandgap + exciton energy.

behavior is observed for metals and insulators. The predominant loss mechanism in metals also for low energies is electron-electron scattering. For electrons in insulators with an energy smaller than bandgap plus exciton energy, electron-phonon scattering is the dominant loss channel [HSt78], a mechanism that is less effective than electron-electron scattering. Thus, a much larger mean free path results. In this work, a mean free path of 60 Å was determined for HeI (21.2 eV) excited photoelectrons from the valence band of CaF_2. The steep increase of the mean free path for low energy electrons in wide bandgap insulators results in a larger sampling

depth for UPS with 21.2 eV photons than for XPS with Al Kα (1486 eV) or Mg Kα (1253 eV) lines. This is the opposite situation to that found in metals. As an estimate, the value of 60 Å determined in this work for HeI excitation may be compared to the mean free path of photoelectrons with typical energies after Al Kα excitation (C1s: 1203 eV, Ca2p. 1140 eV, O1s: 955 eV, F1s: 801 eV) extracted from Fig. 2.13. It is usually stated that the sampling depth of UPS with 21.2 eV excitation is about 5 to 10 times larger than for excitation with typical XPS photon energies provided by laboratory sources. This information will be needed to understand the different observations concerning the cleanness of air cleaved crystals after heating, made with X-ray photoemission and Auger electron spectroscopy on the one hand and with UPS on the other hand.